

We are IntechOpen, the world's leading publisher of Open Access books Built by scientists, for scientists

6,100

Open access books available

149,000

International authors and editors

185M

Downloads

Our authors are among the

154

Countries delivered to

TOP 1%

most cited scientists

12.2%

Contributors from top 500 universities



WEB OF SCIENCE™

Selection of our books indexed in the Book Citation Index
in Web of Science™ Core Collection (BKCI)

Interested in publishing with us?
Contact book.department@intechopen.com

Numbers displayed above are based on latest data collected.
For more information visit www.intechopen.com



Dimensioning of Fractal Fracture on a Concrete Slab

Francisco Casanova-del-Angel

Abstract

What is presented here is a methodology that allows to study fractures in any material, especially in concrete elements. The importance lies in the moment in which the fracture that occurs in a structural element (slab in our case study) causes a negative effect on its structural behavior. Traditionally, its study is developed from the perspective of fracture mechanics, with which the energy at the tip of the crack or fracture is calculated, and it cannot go further. But the combination of the theories of fracture mechanics and fractal geometry allows us to obtain the patterns of its behavior in the future. Thus, the research was based on tests made on structural elements of concrete, from a slab led to structural failure and choosing a fracture. This was vectorized in order to obtain a fractal axis, which was called state 0, taking three parts or sections of that state and repeating them on a smaller scale. Subsequently, the research was based on five of the methods used for the study and calculation of the fractal dimension: box dimension, perimeter-area dimension, information dimension, mass dimension, and ruler dimension. Most of the fractal dimensions obtained under these methods were similar to each other.

Keywords: curved fractal, mechanical fracture, dimension of fracture, concrete, fractal geometry

1. Introduction

I think it is necessary to start this article with some comments that have to do with the icon that represents a fracture, fraction, and the concept of fractal. For those seasoned in fractures and fractals, they can be childish, but not for architects and civil engineers. Why this brief comment? Well, the research covers two gigantic areas of knowledge: fractals and fracture mechanics. The molecular composition in humans, that is, small structures in large quantities, is the same in a single being. Geometric shapes with the same structure, which if split into equal parts, result in the same smaller part that remains the same or many of them to create a larger one with the same features.

A fractal is a geometric object with a basic structure, whether fragmented or irregular, repeated at various scales. Mathematically, a fractal may be expressed as follows: Let $I = [0, 1]$ and let $A_1 = I - (\frac{1}{3}, \frac{2}{3})$ be that subset of I obtained by removing those points which lie in the open middle third of I ; that is, $A_1 = [0, \frac{1}{3}] \cup [\frac{2}{3}, 1]$. Let A_2

be that subset of A_1 obtained by removing the open middle third of $[0, \frac{1}{3}]$ and of $[\frac{2}{3}, 1]$. Continue this process and define A_3, A_4, \dots . The set $C = \cap_{n=1}^{\infty} A_n$ is called the Cantor set. Some characteristics are (i) C is a compact set having Jordan content zero, (ii) C is uncountable, and (iii) the characteristic function of C is Riemann integrable on $[0, 1]$, see [1].

We should bear in mind that the fractal dimension may be calculated in various ways. One is through the Hurst exponent: many structures in nature have the feature to be originated in two dimensions and end in a fractional dimension between two and three [2, 3]. A fractal object should have at least one of the following features: (i) it should show similarity among details on small and large scales; (ii) it should not be able to be represented through classical geometry; (iii) it should have a fractional dimension, that is, a non-whole dimension; and (iv) it should be able to be recursively defined; see [4].

The classical theory of fracture mechanics allows to predict the quick propagation of a macro crack through a homogeneous, isotropic, and elastic material. In this theory, the stress intensity factor, K_I , which is a function of the geometry of the crack and stress, is applied. Failure occurs when K_I reaches a critical value K_{IC} , known as the critical stress intensity factor in plane strain conditions. Therefore, K_{IC} is a measure of the fracture hardness of the material. To properly measure K_{IC} in a material, the sample to be examined must be of a size that allows the ensuring of maximum restriction (plane strain) on the tip of the crack. To apply linear elastic fracture mechanics (LEFM), the value of K_{IC} must be a constant of the material, regardless of the geometry of the specimen (as are other constants of materials, such as yield strength).

Regarding the material used in the laboratory, it must be said that it has the adhesion and cohesion properties required to bond inert aggregates and make a solid mass with proper resistance and durability, as well as that for the fabrication of structural concrete the so-called hydraulic cements are exclusively used. In the current case, Portland cement has been used since it is a grayish material finely powdered, mainly formed by calcium aluminum silicates, see [5, 6]. When the cement is mixed with water to create a soft paste, it gradually becomes rigid until becoming a solid mass. This process is known as casting and hardening.

2. Laboratory tests

The test included applying a load concentrated on the gravity center of a 70 cm wide and 500 cm long portion of a prefabricated slab, 20 cm thick with two open web joists on the ends and a small vault covering the span, **Figure 1**. The test required the construction of a slab portion, 70 cm wide and 500 cm long with two joists on the ends and small vaults covering the spaces between them, with a 6*6–10/10 electro-welded mesh and a 3 cm thick concrete layer in the compression zone. The slab was supported by two 70 cm long and 170 cm high concrete blocks, low walls with reinforcing bar grids, and closure slabs armored with *armex* 15*20–4, while to confine such low wall headframes were placed on the ends with *armex* 15*20–4. The resistance to the compression of the concrete was 200 kg/cm², see [7].

The steel required for the area was calculated for the construction of the 5 m long joist, with a 17 cm slope. Once the steel areas were obtained, preassembling, armoring, and casting of the joints were carried out together with the curing process, waiting for



Figure 1.
View of the slab before the first load.

the concrete to reach its maximum strength. The joints and the small vaults were taken to the laboratory where the load frames were placed to place the prefabricated slab. First, the low walls to support the slab were constructed with a concrete block, founded on a reinforcing bar grid with a 15 cm base and 20 cm slope, and armored with *armex* 15*20–4. To confine the low wall, headframes were placed on the ends, 15 cm by 20 cm, armored with *armex* 15*20–4, and the same was used for the closure slab. After that, the required formwork was placed, the joists were fitted into the closure, and the small vaults were put in place. In the center of the span, a temperature nerve was placed and for the compression layer a 6*6–10/10 electro-welded mesh was used and a 3 cm thick layer was placed at the closure, allowing the concrete to harden, *ibid*.

After 7 days, the formwork was removed from the slab, the concrete having been cured for days previously. After this and after the concrete reached its maximum strength, which occurred 28 days after casting the slab, the test started. To be precise in obtaining the results, the load cell was first calibrated in the computer. To do this, a wooden pole was placed on which the load was applied. In the computer, it was observed if the load and strain were registered, which were correct. Then, the load was taken away and all data involved in the test were marked as zero. A smooth steel rod was placed on the central axis of the slab and with such a steel a square profile was placed to reach the height of the frame load piston, which in turn supported the 200-ton load cell. At last, we have the piston applying the load on the frame. Under the slab and on the sides of the low walls supporting the slab, micrometers were placed to measure warping and lateral strain. To easily observe the cracks, the slab's lower part was painted white.

To start, a 10-ton load was applied. When the first cracks appeared, they were colored with a green marker. Then, a second 10-ton load was applied. New cracks appeared and the existing ones were enlarged. Those were colored with a red marker. A 5-ton load was then applied. More cracks appeared and the existing ones were



Figure 2.
Evolution of cracking as the load was applied.

enlarged, which were then colored blue. Finally, a final 5-ton load was applied. No new cracks appeared, only the existing ones were enlarged. Those were colored brown. Days after that, the test was continued applying load until the slab collapsed, **Figure 2**.

3. Fractal dimension

In fractal geometry, the fractal dimension D is a real number that generalizes the concept of ordinary dimension for geometric objects that do not admit tangential space and is an exponent, which accounts for the wholeness, that seems to fill a fractal in space as it moves toward finer and finer scales. The problem here is that there exists a series for its calculation which frequently but not always is equivalent. Among the ones mostly used are: Hausdorff-Besicovitch dimension, packing dimension, homothetic dimension, and Rényi dimensions. None of these is universally used, and one of the reasons for this is that the discrepancy among them is related to differences in the structure of the fractal. Although for a great number of classical fractals the values of the various definitions of fractal dimension and all those dimensions coincide, they are not equivalent. The positive aspect of this is that some definitions of fractal dimension are easy to calculate and are probably more used. However, they do not always have the most desirable mathematical properties.

3.1 Dimensioning of fractal fracture on a concrete slab

In the study of fractures, from a fractal point of view, the previously specified slab was used, **Figure 1**, on which loads were applied. Propagation of the crack depends on important factors, such as stress and intensity. It also depends on the curing of concrete and the resistance of such structural elements. To carry out such dimensioning of the slab on which loads were applied, a crack was chosen among all cracks

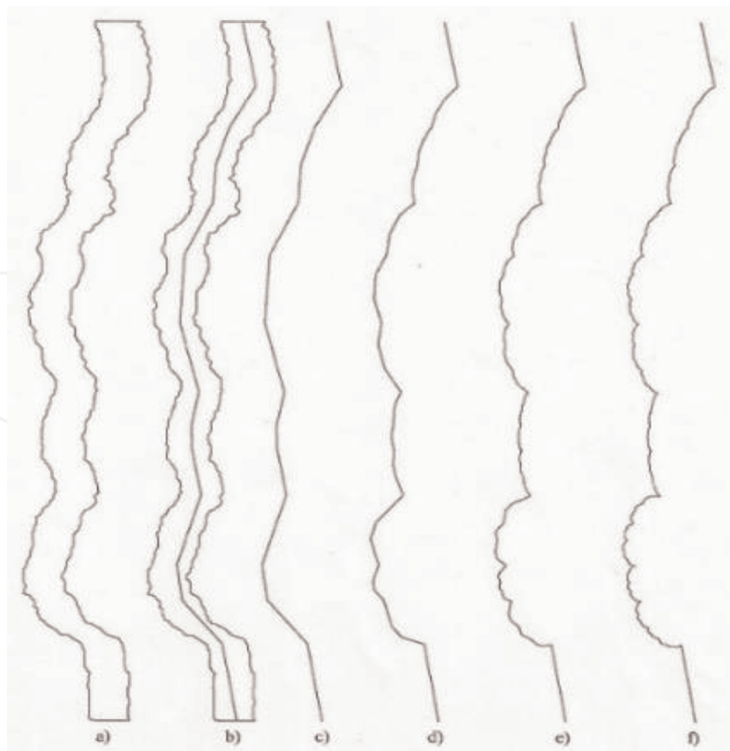


Figure 3. (a) Vectorization of the (b) image with fractal axis and 4 fractal radius increases statuses of the fracture; (c), (d), (e), and (f) (Statuses 0, 1, 2, and 3).

created and vectorization of the outline of the chosen fracture was carried out, **Figure 3a**, with CorelDraw 4X to obtain the axis of the fracture.

From here, a set of parts of that axis was sectioned and chosen to create the generator, which will be known as the starting point of the fractal. In this case, three strokes were chosen, which are constantly repeated throughout the fracture, **Figure 3a** and **b**. These strokes are repeated at a lower scale than the original one, within each separate section, called status. The main axis of the fracture is *status 0*, following scale or lower repetition, *status 1*, and so on, repeatedly, up to *status n*. In this study, we only used up to *status 3* of the fracture, since the scale with higher status becomes imperceptible. These repetitions at a lower scale were made with AutoCAD software.

Upon obtaining *status 0*, certain symmetry and proportionality were observed in the fracture. It showed a 70° tilt degree and a proportional radius increment in circles as the length of the fracture increased, **Figure 4**. Upon meshing with the vertical and horizontal axes, regarding the tilt of the radius increasing angle, it was observed that *Status 0* matched with the beginning and the end of the vertical axis and that the increments in radius upon writing X against Y showed almost the same proportion, **Figure 4**. After this process, the fractal dimension for each status was calculated using five of the well-known theoretical methods: (i) box dimension, (ii) perimeter-area dimension, (iii) information dimension, (iv) mass dimension, and (v) ruler dimension. The fundamental explanation for why all these methods were used for the calculation of the fractal dimension of the fractured slab is that each method provides different results for the fractal dimension of the fracture, and it has been wanted to manifest that the values obtained are very similar but slightly different. To estimate the fractal dimension, a fractal dimension calculator should be used, and this is carried out through the algorithm *box-counting* or *box-counting dimension*.

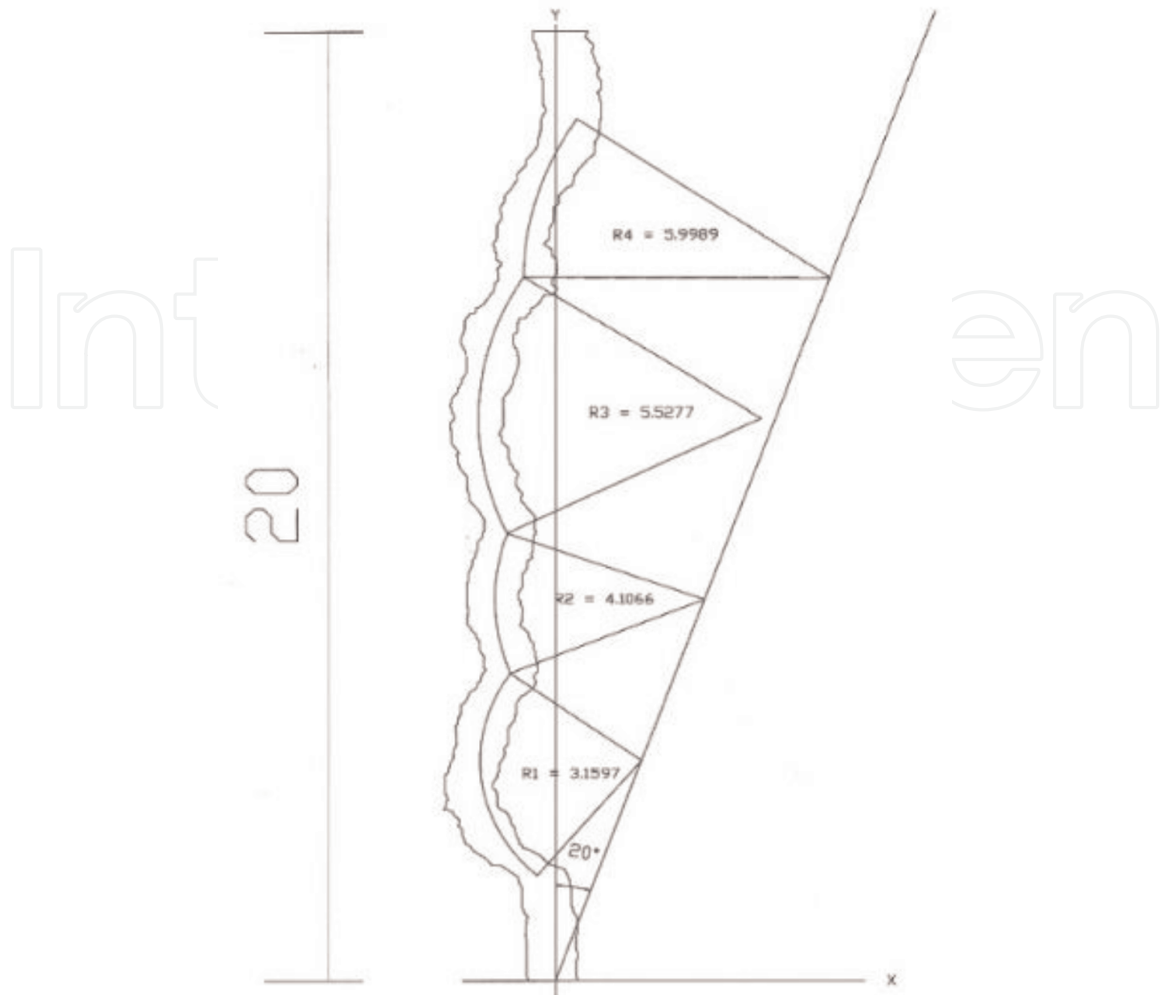


Figure 4.
Fracture tilt angle.

3.2 Fractal dimension through the box-counting method (box-dimension method)

This is an application created in the beginning of the 1990s. It establishes that if a line is split in half, we will have two parts to recreate the original line. If it is split into four parts, we will use that to cover the original line. We may deduce that if we split a line's time, we will have such a number of segments covering the original line. Therefore:

It is also true that, if we take a square and split each side in half, we obtain four smaller parts of the original square. If we split each side into $\frac{1}{4}$, we will have 16 parts of the original. Therefore, if we repeat this for: $D = 2 : N_s = \left(\frac{1}{s}\right)^2$ and for $D = 3 : N_s = \left(\frac{1}{s}\right)^3$.

1, 2, and 3 exponents in the above examples are fundamental for the concept of dimension. This may be generalized by Eq. (1):

$$N_s = \left(\frac{1}{s}\right)^D \quad (1)$$

Fractal dimension	Standard deviation	R-square	Equation of straight line	Estimation method
1.95322	0.0109513	0.9964	$y = 1.81E+06 * x^{-1.95}$	Box dimension
1.03266	0.1647710	0.9855	$y = 0.105 * x^{1.94}$	Perimeter-area dimension
1.96417	0.0010445	0.9921	$y = 1.78E+06 * x^{-1.96}$	Information dimension
1.95776	0.0093884	0.9898	$y = 3.9 * x^{1.96}$	Mass dimension
1.01606	0.0009957	0.9823	$y = 6.14E+03 * x^{-1.02}$	Ruler dimension

Table 1.
 Values of calculation of fractal dimension for each method used.

where D is the dimension (whole or unit) as in the beginning, but if we take logarithms on both sides, we have Eq. (4):

$$\log(N_s) = D \log\left(\frac{1}{s}\right) \quad (2)$$

In other words, we may estimate the dimension graphing $\log(N(s))$ to $D \log(1/s)$. Its slope is the dimension. If the said dimension is not a whole, then it is a fractioned dimension.

The box-dimension method is the most popular one and counts boxes containing part of the fractal as a calculation procedure. Given an A fractal structure contained in a d -dimensional volume, the counting method implies distributing the space of the structure on a fixed d -dimensional mesh with square boxes of the same size r . Several algorithms [8–10] based on this method have been widely developed and used to estimate D_f , and may be applied to systems with or without self-similarity. The fractal dimension obtained was 1.95322, **Table 1**.

3.3 Fractal dimension through the perimeter-area dimension method

The perimeter-area fractal dimension is attractive because it reflects the complexity of a shape through a range of spatial scales (size of fragments). However, as it's homologous to the fragment level (FRAC), the perimeter-area fractal dimension is only significant if the log-log ratio between perimeter and area is linear on the full range of fragment sizes. If it is not (and this should be determined separately), the fractal dimension is calculated separately for the range of patch sizes or fragments on which it is constant. Note that as this index uses regression analysis, it is subject to false results when there are small sample sizes. In mosaics with only some patches or fragments, it is common to obtain values above the theoretical limits of this index. PAFD (perimeter-area fractal dimension) is equal to 2, divided by the slope of the regression line obtained through regression of the mosaic piece mosaic area logarithm (in square meters) times the piece mosaic perimeter logarithm (in meters). That is, 2 divided by the coefficient b_1 derived from a regression of minimal squares for the equation $\ln(\text{area}) = b_0 + b_1 * \ln(\text{perimeter})$. Note that PAFD excludes any background mosaic. It has no units and its range is $1 \leq \text{PAFD} \leq 2$.

The formula for the calculation of the fractal dimension through this method is Eq. (5).

$$PAFD = \frac{2}{\frac{\left[n_i \sum_{j=1}^n (\ln(p_{ij}) * \ln(a_{ij})) \right] - \left[\left(\sum_{j=1}^n \ln(a_{ij}) \right) \left(\sum_{j=1}^n \ln(p_{ij}) \right) \right]}{\left(n_i \sum_{j=1}^n \ln(p_{ij}^2) \right) - \left(\sum_{j=1}^n \ln(p_{ij}) \right)^2}} \quad (3)$$

a_{ij} is the area (in square meters) of the fragment or piece ij , p_{ij} is the perimeter (in meters) of the fragment or piece ij , and n_i is the number of pieces in the mosaic patch or fragment i (class). The fractal dimension thus obtained is 0.164771, **Table 1**.

3.4 Information-dimension method

The concept of fractal dimension may be seen as a basic vision of complex construction. Let us define the information function as Eq. (6), see [11]:

$$I = - \sum_{i=1}^N P_i(\epsilon) \ln [P_i(\epsilon)] \quad (4)$$

where $P_i(\epsilon)$ is the natural measure or the probability that the element i is the index of the normalized population such that: $\sum_{i=1}^N P_i(\epsilon) = 1$. The dimension of information d_{inf} is Eq. (7):

$$d_{inf} \equiv - \lim_{\epsilon \rightarrow 0^+} \frac{I}{\ln(\epsilon)} = \lim_{\epsilon \rightarrow 0^+} \sum_{i=1}^N \frac{P_i(\epsilon) \ln [P_i(\epsilon)]}{\ln(\epsilon)} \quad (5)$$

The fractal dimension, thus obtained is 0.0010445, **Table 1**.

3.5 Mass-dimension method

Unifractal shows something similar to a random Cantor dust. This is the version of the two dimensions of the Cantor set, attributed to the mathematician George Cantor [12]. The method was supported when Berger and Mandelbrot found data showing strong hierarchical grouping in a high number of superimposed levels. The model published is a discretized Lévy dust, but the authors here consider the first a model based on Cantor dust, see [13].

Entries N and b are not present in more realistic models, much less in reality, and should not be measured separately only through the similar dimension Eq. (8).

$$D = \frac{\log N}{\log b} \quad (6)$$

In the case of Lévy dust, no counter-physical grid and cascade are involved; hence, N and b are not needed. Here, the sole parameter D is an easily measurable concrete quantity. It is not a similarity dimension, but a mass dimension. That is, an interval of length R centered on the dust contains a mass of the order of R^D . The fractal dimension obtained with this method is 0.0093884, **Table 1**.

3.6 Ruler-dimension method

A standard method used to estimate the length of a curve in a plane is counting how many lengths of a ruler are used to move from the start to the end of the curve. Since the ruler has a finite length, the details of the curve are smaller than the ruler with which we obtain the jumps, and therefore, the length we measure is generally lower than the real length. We intuitively believe our rulers are shorter, but our estimation of the actual length is more exact and increases.

The estimation of the length on the right is closer to reality since successive rulers are closer. The estimation improves each time the length of the ruler decreases.

The ruler or compass dimension of a curve is calculated between the ratio of a ruler with length L and the number of rulers required to measure the length of a curve, given as $N(L) = c L^{-D}$, where c is a constant. Taking the logarithms of both sides, we have: $\log(N(L)) = \log(c) - D \log(L)$. Therefore, if we graph $\log(N(L))$ vs $\log(L)$ within a range valued as L , the slope will be an estimate of the fractal dimension D , see [14, 15]. It must also be said that after making the corresponding scaling of *Status 0* of the fracture chosen up to *Status 3*, the necessary calculations were made through the methods mentioned above. The fractal dimension, thus obtained, is 1.01606, **Table 1**.

Table 1 shows that there is a great similarity among three of the methods regarding the results: box dimension, information dimension, and mass dimension; because the fracture is proportional as it expands along the slab. We may observe that the fractal dimension is between 1 and 2. In addition to this, from the values in **Figure 6**, it was

x	Slope equation $y = a + bx$
1.68	4.71675451
2.91	8.16668121
4.02	11.2800297
5.37	15.0665346

Table 2.
 Results of calculation of the slope of fracture radius dot increase.

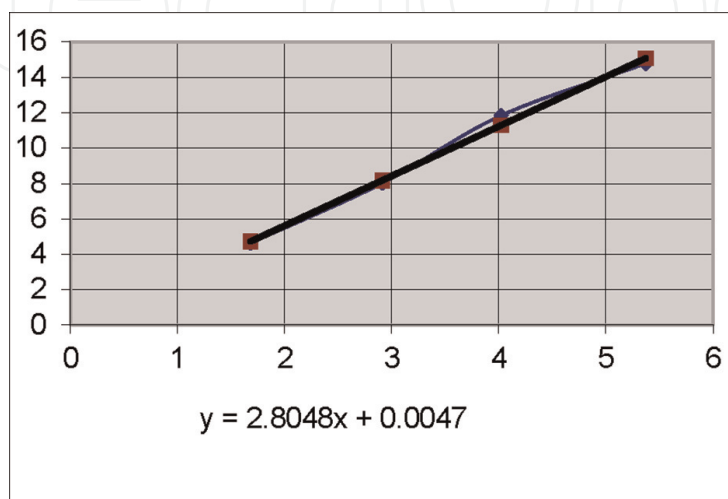


Figure 5.
 Increase in the slope of straight line and equation of the slope.

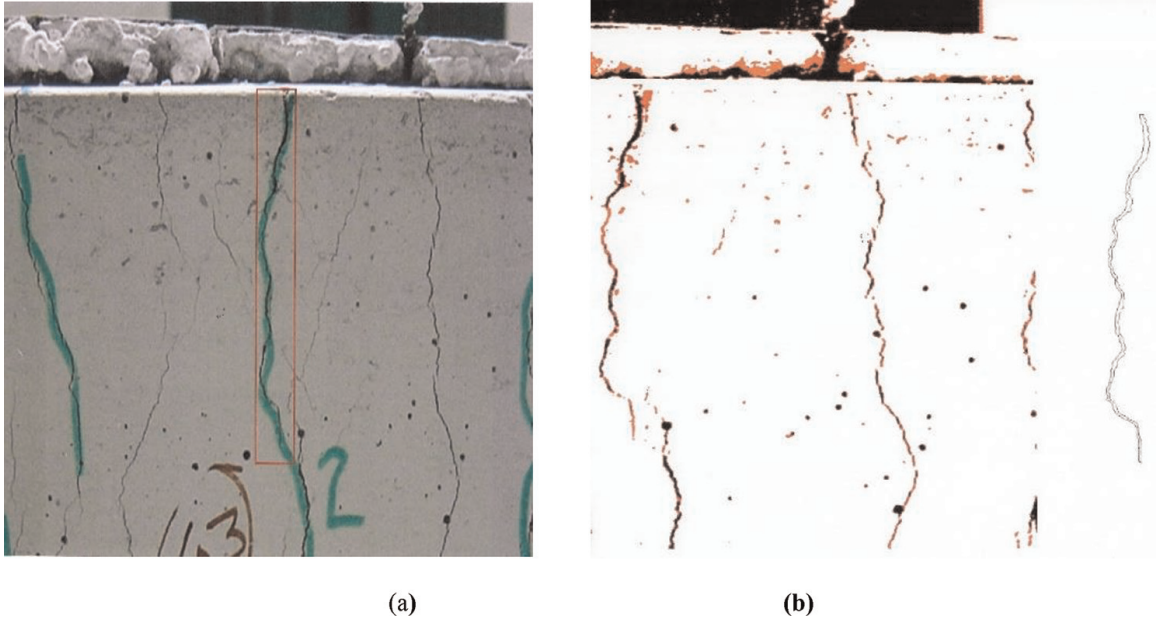


Figure 6.
(a) Fracture chosen and (b) its vectorization.

possible to obtain the equation of the pending line of the increments that the fracture had, **Table 2**. The values obtained are represented in **Figure 5**.

4. Intersection of fractal curves

Let us now focus on a phenomenon commonly present in this type of tests or cases: the intersection of fractal curves, as shown in **Figure 2**. Since the intersection of fractals F and G is often a fractal, it is natural to relate the dimension of such an intersection with one of the original sets, but, in general, it may not be said that A is true. This is because if F is limited, there may exist a copy F_1 of F such that $\dim(F \cap F_1) - \dim F$ exists, but in the copy, if the sets are disjoint, $\dim(F \cap F_1) = \Phi$. In addition, if F and F_1 are collinear, then $F \cap F_1$ is a line segment. However, if they intersect at a given angle (as in **Figure 2**), such an intersection is a singular or sole point (also shown in **Figure 2**). The latter case is the most frequent. If the transformation σ of the plane is congruent; that is, a rigid movement, it transforms any set F into a congruent $\sigma(F)$ without reflection. Rigid movements may be parameterized through coordinates (x, y, θ) , with θ being the rotation angle.

The objective of the study of fractals is to know the dimension of fractal curves intercepted. Since the ways to obtain the fractal dimension are varied, we will use the Hausdorff-Besicovitch dimension (see below), which is based on considering an open cover of n -spheres of the fractal set, that is, for a fractal contained in the Euclidean plane open circles are considered (in mathematics we talk about balls, but everything depends on the dimension in which such exist). Of the possible coatings, the minimum formed by balls with a smaller diameter equal to a given size ε , Eq. (9) is considered. Once such a minimum is calculated, its limit is considered when $\varepsilon \rightarrow 0$, therefore formally defining Hausdorff content as:

$$\mathcal{H}_\delta^\varepsilon(F) = \min \left\{ \sum_{i=1}^{\infty} |U_i|^\varepsilon \right\} \ni \mathcal{H}^\varepsilon(F) = \lim_{\delta \rightarrow 0} \mathcal{H}_\delta^\varepsilon(F) \quad (7)$$

where $|U_i| = \text{diam}(U_i) < \delta$, complying with the fact that Hausdorff content defines a function of the set power \mathfrak{R}^n in non-negative real numbers, Eq. (10).

$$\mathcal{H}^s : P(\mathfrak{R}^n) \rightarrow \{0\} \cup \mathfrak{R}^+ \cup \{\infty\} \quad (8)$$

For any set, the function defined in Eq. (10) has the property to be null for any $s > s_0$ and infinite for $s < s_0$, and for $s = s_0$ the Hausdorff-Besicovitch dimension is obtained, shown below dim_{HB} .

Given F and G are two fractal curves to which the dimension mentioned above has been applied, then, in general, it is true that Eq. (11):

$$\text{dim}(G \cap \sigma(F)) \leq \max\{0, \text{dim}G + \text{dim}F - n\} \quad (9)$$

And it is also true that Eq. (12):

$$\text{dim}(G \cap \sigma(F)) \geq \text{dim}G + \text{dim}F - n \quad (10)$$

Therefore, it is possible to obtain higher limits for $\text{dim}(G \cap \sigma(F))$ with a given translation or similarity group. Such limits are kept for large groups of translations and similarities.

Based on **Figure 7**, and as was mentioned in the first paragraph of this section, parameterization allows a natural measure in the space where the rigid movement is made with the measure of a rigid movement set given in space, for instance, tridimensional, and if we assign the origin to a certain point in the rectangle $[1, 2] \times [0, 2]$ we obtain measure $1 \times 2 \times 2\pi$.

Algebraically, in \mathfrak{R}^n where two smooth variables G and F are completely intersected, in general, they intersect in a sub-variety of dimension $\max\{0, \text{dim}G + \text{dim}F - n\}$. If $\text{dim}G + \text{dim}F - n > 0$, therefore Eq. (13):

$$\text{dim}(G \cap \sigma(F)) = \text{dim}G + \text{dim}F - n \quad (11)$$

For a rigid movement set with positive measure, but it is 0 for everything else.

The study of fractal intersections moving between them is known as integral fractal geometry. In the optics of classical geometry, see [16], they may be

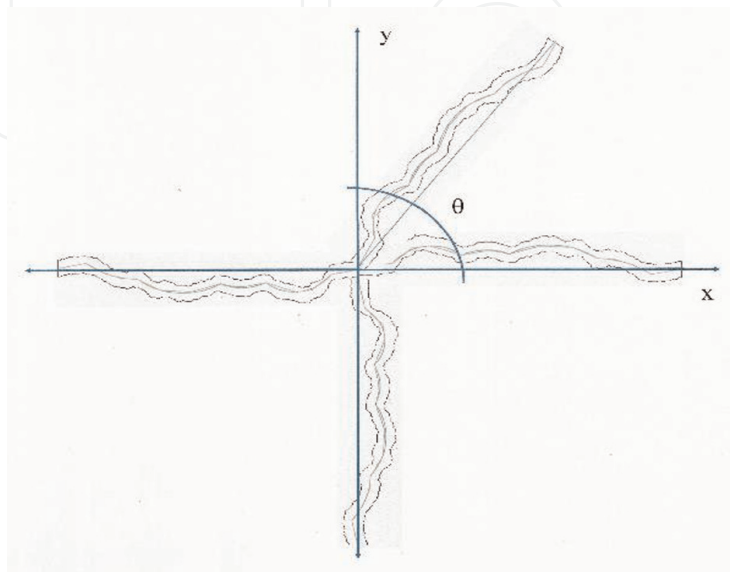


Figure 7.
 Intersection of fractals.

consulted, and the ones who have contributed the most to the fractal intersection are seen [17–20].

Although the vectorization of the fractal image was chosen here, there is an article that proposes a method of rapid fractal coding based on the fractal dimension. The fractal dimension in fractal theory can be used to describe the texture of the image. The larger the fractal dimension, the rougher the surface of the corresponding graph, and vice versa. The method is based on the differential box count that is chosen specifically for texture analysis. Since the search space is reduced and the sorting operation is simple and computationally efficient, improving the encoding speed and preserving the quality of the decoded image; see [21].

5. Conclusions and impact of the research

From the civil engineering point of view and regarding the laboratory tests, it must be established that the low walls supporting the slab bent within the permissible limits since there were already headframes confining them. On the other hand, there was no reinforcing steel in the temperature nerve, so it did not function as such and that was a noticeable aspect. In addition, the surface of the slab on which the smooth steel rod was placed was not smooth enough, that is, the surface of the slab was rugose, which caused the load again not to be completely vertical, but rather, that the load might have had a certain unknown tilt angle but is supposed to be lower than the angle generated in the first test, so that applied load may be diminished in a certain percentage lower than the previous one. Taking into account the deformations obtained in this test, they were also higher than the permissible ones, above all, in the second and third loads. In the first test, it was almost the permissible one: 2.61, 4.73, and 5.98 cm, respectively.

The element worked satisfactorily, and while it is true that its deformations were not permissible, this was because the loads applied are not the ones usually received by a slab, and in cases where it is necessary to support a load of such magnitude, it has to be replaced with an element with higher load capacity, such as a slab or if necessary a column, **Figure 8**.

Regarding the fractal part, the methods used in this work are related to the fractal line or curve taken as a unit and the number of segments into which it is divided and the fractal dimension is always between one and two, but not higher than two. Logarithmic units are used, since smaller scales of the unit are progressively used, which are proportionally mirrored, that is why the logarithm is used, due to the smaller proportionate scales that appear. In the equations of straight lines shown in **Table 1**, we may see that the exponents to which the variable x is raised are almost identical, except for the one obtained through the ruler-dimension method.

Whether using the box-dimension method, the ruler-dimension method, or the mass-dimension method, these methods are related to the logarithm of N (which is the unit or the whole of a segment) between the numbers of s (which is the number of parts into which N is divided).

The increase of regression lines has also been observed, but they do not change since they follow the same increase direction. This means that the fracture never gets to failure, which will increase infinitely at higher scales, and which, to the eye, one might think is a curve, but from a closer point of view, one would realize that there are the same fractal lines but very small. These are imperceptible to the human eye and are only visible through other instruments or programs that may increase the scale of



Figure 8.
Large deformation and cracking a short time before the collapse.

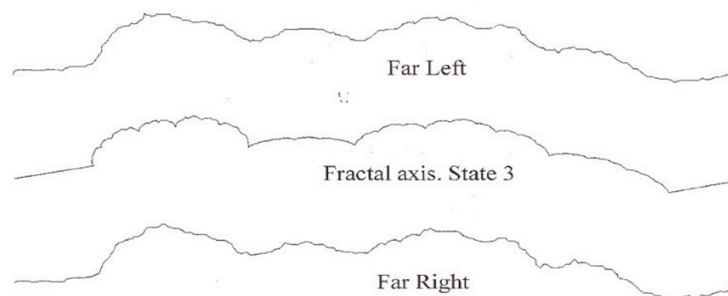


Figure 9.
Comparison of the ends with the fractal axis in its status 3.

the drawing. In addition, it has been observed that *Status 3*, which is still the fractal axis but at a higher scale, shows us that it is very similar to the borders of both ends, which at a higher scale would be more similar to the fractal axis, with a higher *status n* on the borders of the fracture. This shows that no matter the distance of the opening of the fracture, it will always be the same and/or similar to the fractal axis on both ends, **Figure 9**.

Regarding the theoretical part related to the fractal intersection, it has been proven that if there are two collinear fractal curves, their intersection is a segment of a line. If they are cut with a certain angle, **Figure 2**, such an intersection is a singular point and the rigid movements may be parameterized through coordinates (x, y, θ) ; with θ being the rotation angle. In addition, the fractal geometry obtained with the fractal in **Figure 3** is impressive upon considering the large intersections between them.

Acknowledgements

I want to thank Velasco Aguilar, C. S., and Casanova-del-Angel, F., who have allowed me to use one of the different tests carried out on various reinforced concrete

structures (columns, beams, slabs, and frameworks), published in [10]; Santos Vázquez, R. E., who has made some of the calculations to dimension the fracture under study [22]; and the IPN-SIP research projects 20181253 and 20196119.

Conflict of interest


The author declares no conflict of interest.

Author details

Francisco Casanova-del-Angel
ESIA, Unit ALM of the Instituto Politécnico Nacional. Mexico

*Address all correspondence to: fcasanova49@prodigy.net.mx

IntechOpen

© 2022 The Author(s). Licensee IntechOpen. This chapter is distributed under the terms of the Creative Commons Attribution License (<http://creativecommons.org/licenses/by/3.0>), which permits unrestricted use, distribution, and reproduction in any medium, provided the original work is properly cited. 

References

- [1] Apostol Tom M. *Mathematical Analysis: A Modern Approach to Advanced Calculus*. Department of Mathematics. California Institute of Technology. Addison-Wesley Publishing Company Inc; 1965
- [2] Hurst HE. Long-term storage capacity of reservoirs. *Proceedings of the Institution of Civil Engineers*. 1951;**116**: 770-808
- [3] Hurst HE, Black RP, Simaika YM. *Long-term Storage: An Experimental Study*. London: Constable; 1965
- [4] Barnsley M. *Fractals Everywhere*. Orlando, FL: Academic Press Inc; 1988
- [5] ASTM C150/C150M-12. *Standard Specification for Portland Cement*. West Conshohocken, PA: American Society for Testing and Materials International; 2012
- [6] Wang L, Jin M, Zhou S, Tang S, Xiao L. Investigation of microstructure of C-S-H and micro-mechanics of cement pastes under NH_4NO_3 dissolution by ^{29}Si MAS NMR and microhardness. *Measurement*. 2021;**185**:110019
- [7] Velasco Aguilar CS, Casanova-del-Angel F. Estudio de las fracturas con fractales en elementos de concreto reforzado: pruebas de laboratorio. *Journal El Portulano de la Ciencia*. 2004;**12**:421-434
- [8] Li J, Du Q, Caixin S. An improved box-counting method for image fractal dimension estimation. *Pattern Recognition*. 2009;**11**:2460-2469
- [9] Nirupam S, Chaudhuri BB. An efficient differential box-counting approach to compute fractal dimension of image. *IEEE Transactions on Systems, Man, and Cybernetics*. 1994;**24**(1): 115-120
- [10] Pentland AP. Fractal-based description of natural scenes. *IEEE Transactions on Pattern Analysis and Machine Intelligence*. 1984;**6**: 661-674
- [11] Baker GL, Gollub JB. *Chaotic Dynamics: An Introduction*. 2nd ed. Cambridge, England: Cambridge University Press; 1996
- [12] Cantor G. On the power of perfect sets of points (De la puissance des ensembles parfait de points). *Acta Mathematica*. 1884;**4**:381-392
- [13] Berger JM, Mandelbrot BB. A new model for error clustering in telephone circuits. *IBM Journal of Research and Development*. 1963;**7**(3):224-236
- [14] Otto PH, Richter PH. *The Beauty of Fractals*. Germany: Springer-Verlag; 1986
- [15] Peitgen HO, Jürgens H, Saupe D. *Fractals for the Classroom: Part One Introduction to Fractals and Chaos (Corrected Edition)*. Springer 1991. ISBN-10: 038797041X. ISBN-13: 978-0387970417
- [16] Santaló LA. *Integral Geometry and Geometric Probability*. Reading, MA: Addison-Wesley; 1976
- [17] Kahane JP. *Aspects of Mathematics and Its Applications*. Amsterdam: North-Holland; 1986. pp. 419-430
- [18] Mattila P. Hausdorff dimension and capacities of intersections of sets in n -space. *Acta Mathematica*. 1984;**152**: 77-105

[19] Mattila P. On the Hausdorff dimension and capacities on intersections. *Mathematika*. 1985;**32**: 213-217

[20] Mattila P. *Geometry of Sets and Measures in Euclidean Spaces*. Cambridge: Cambridge University Press; 1995

[21] Wang X-Y, Lang Y. A fast fractal encoding method based on fractal dimension. *Fractals*. 2009;**17**(04): 459-465

[22] Santos Vázquez RE. Dimensionamiento de la fractura fractal en el concreto [Tesis de licenciatura]. Mexico: Escuela Superior de Ingeniería y Arquitectura, Profesional Unit Adolfo López Mateos of the Instituto Politécnico Nacional; 2016